Journal of the Korean Physical Society, Vol. 58, No. 6, June 2011, pp. 1672∼1676

Synthesis of Barium Ferrite for Visible Light Photocatalysis Applications

P. H. Borse
Center for Nanomaterials, International Advanced Research Center for Powder Metallurgy and New Materials (ARC International), Balapur PO, Hyderabad, AP 500 005, India

C. R. Cho
Department of Nano Fusion Technology, Pusan National University, Miryang 627-706, Korea

K. T. Lim
Department of Imaging System Engineering, Pukyong National University, Busan 609-735, Korea

Y. J. Lee, T. E. Hong, J. S. Bae, E. D. Jeong, H. J. Kim and H. G. Kim*
Korea Basic Science Institute, Busan 609-735 and Daejeon 305-333, Korea

(Received 30 March 2011, in final form 26 April 2011)

Orthorhombic phase $BaFe_2O_4$ powder was synthesized by using a solid state reaction method and investigated for its visible light photocatalytic properties. The crystallization of the structural phase was found to occur at a temperature above 1000 °C yielding a pure orthorhombic phase $BaFe_2O_4$ (SG- B $b21m$) at 1100 °C. The estimated band gap, as determined by UV-Vis diffuse reflectance studies, was ∼1.9 eV (652 nm). A new material was designed and fabricated as $Pt/RuO_2/BaFe_2O_4$ to enhance its photocatalytic activity. A very low (<1 wt% RuO_2) co-catalyst doping over $BaFe_2O_4$ was important for achieving high photocatalytic efficiency. The newly designed system was investigated for photo-decomposition of isopropyl alcohol (IPA) and of water under visible light (≥420 nm). Its photocatalytic activity was significantly higher than that of platinized $TiO_{2-x}N_x$. A mechanism has been proposed to explain the photocatalytic behavior of the designed $BaFe_2O_4$ photocatalyst.

PACS numbers: 81.61.Fn, 81.05.Zx, 85.40.Zx
Keywords: $BaFe_2O_4$, Solid state reaction, Visible light, Photocatalytic activity, Photodegradation
DOI: 10.3938/jkps.58.1672

I. INTRODUCTION

Presently, the whole world is attempting to discover an eco-friendly, stable and efficient visible-light photocatalyst for producing hydrogen by water splitting, as it is one of the potential ways to generate the desirable renewable energy. The progress in the photocatalysis research during the last decade was limited to the ultraviolet (UV) light region although the visible light region of electromagnetic spectrum is far more abundant and useful for an efficient photocatalysis under solar light. Several research groups have developed visible active oxide, sulfide and oxynitride photo-catalysts such as $PbBi_2Nb_2O_9$, $(Ga_{1-x}Zn_x)(N_{1-x}O_x)$, $Ni_xIn_{1-x}TaO_4$, TaON, $TiO_{2-x}N_x$, $TiO_{2-x}C_x$, $Sm_2Ti_2O_5S_2$, $AgGa_{1-x}In_xS_2$, *etc* [1-9]. Recently, we discovered a few novel photocatalysts, *viz.* an Aurivillius-phase $PbBi_2Nb_2O_9$ perovskite, its nano-composite, its modified form of a *p-n* junction nano-diode, *etc.* [10-14], as efficient photocatalysts working under visible light. However, there is still a need for a highly efficient, small band gap (*ca.* $E_g = 1.9 \sim 2.1$eV) photocatalyst, that will absorbs visible light photons from the solar spectrum. Barium mono ferrite ($BaFe_2O_4$), an orthorhombic phase, low-band-gap ferrite material, thus has become a crucial candidate for visible light photo-catalysis. In past, its applications in magnetism, paints and pigment and catalysis have been demonstrated [15]. These properties are due to the existence of Fe ions in the lattice with tetrahedrally/ octahedrally coordinated ligands. This not only affects the metal-ion spin dynamics but also renders visible-light absorptivity to the material. Similar to $CaFe_2O_4$, this metal oxide is a *p*-type semiconductor and is thus suitable for the photodegradation of organic pollutants [16]. In order to explicitly confirm this, we have investigated the photocatalytic performance of this material. We have studied the CO_2 production from the photo-degradation of iso-propyl alcohol (IPA), it being a role model pollutant. Further, we have also investigated

*E-mail: hhgkim@kbsi.re.kr; Tel: +82-51-974-6104; Fax: 82-51-974-6116

the photo-reduction of water from water-methanol mixtures under visible light irradiation ($\lambda \geq 420$ nm). As a part of the above investigations, we have characterized nanocrystalline $BaFe_2O_4$ for its optical and structural properties, respectively, by using an UV-vis diffuse reflectance spectrometer and an X-ray diffractometer. This exploratory study demonstrate the feasibility of using $BaFe_2O_4$ for photodecomposition of C_3H_7OH and H_2O.

II. EXPERIMENTAL

The orthorhombic $BaFe_2O_4$ photocatalyst was synthesized by using the conventional solid state reaction (SSR) method. Stoichiometric amounts of $BaCO_3$ (99.7%, Aldrich) and Fe_2O_3 (99.9%, Aldrich) were mixed and ground in methanol to obtain a homogeneous mixture. The pelletized powders were subjected to calcination at various temperatures in the range of 1100 °C - 1300 °C for 5 h in a static furnace. In an additional experiment, nanoparticle $TiO_{2-x}N_x$ powder was also prepared as a standard visible-light-active photocatalyst by using the hydrolytic synthesis method (HSM) [17]. In this synthesis, an aqueous ammonium-hydroxide solution with an ammonia content of 28 - 30% (99.99%, Aldrich) was added drop by drop to a 20% titanium (III)-chloride solution ($TiCl_3$, Kanto, containing 0.01% iron as the major impurity) for 30 min under N_2 flow in an ice bath while continuously stirring. Later, the suspension was further stirred for 5 h to complete the reaction. After completion of the reaction, the precipitate was filtered in air and washed several times with deionized water. The filtered powder was dried at 70 °C for 3 - 4 h in a convection oven. The sample obtained at this stage was an amorphous powder containing ammonia and titanium species. Further, this sample was calcined at 400 °C for 2 h in air flow in an electric furnace. This yielded the desirable crystalline $TiO_{2-x}N_x$ powder.

The $BaFe_2O_4$ samples were characterized by using an X-ray diffractometer (Mac Science Co., M18XHF). X-ray diffraction (XRD) results were compared with the Joint Committee Powder Diffraction Standards (JCPDS) data for phase identification. The optical properties, mainly the band gap energies of the as-prepared materials, were estimated by using an UV-Visible diffuse reflectance spectrometer (Shimadzu, UV 2401). The particulate morphology was characterized by using scanning electron microscopy (SEM, Hitachi, S-2460N). A detailed structural characterization was carried out by using high-resolution transmission electron microscopy (HR-TEM, Philips, CM 200).

For all the samples, the photocatalytic degradation of iso-propyl alcohol (IPA) was studied to estimate the photocatalytic activities under visible-light irradiation ($\lambda \geq 420$ nm). About 200 ppm of gaseous iso-propyl alcohol (IPA) was injected into a 500-mL Pyrex reaction cell filled with air and 0.3 g of the catalyst. The concentration of the reaction products (CO_2) was determined by using a gas chromatograph equipped with a thermal conductivity detector (TCD) and CTR 1 packed column. Before the reactions, 0.5 wt% of Pt was deposited on the photocatalysts by using the photo-deposition method under visible light ($\lambda \geq 420$ nm). In addition, the photoreduction of water was studied under visible-light photons. We estimated the rate of hydrogen evolution from the half cell reaction of water splitting in the water-methanol solution. The H_2 concentration was analyzed by using gas chromatography.

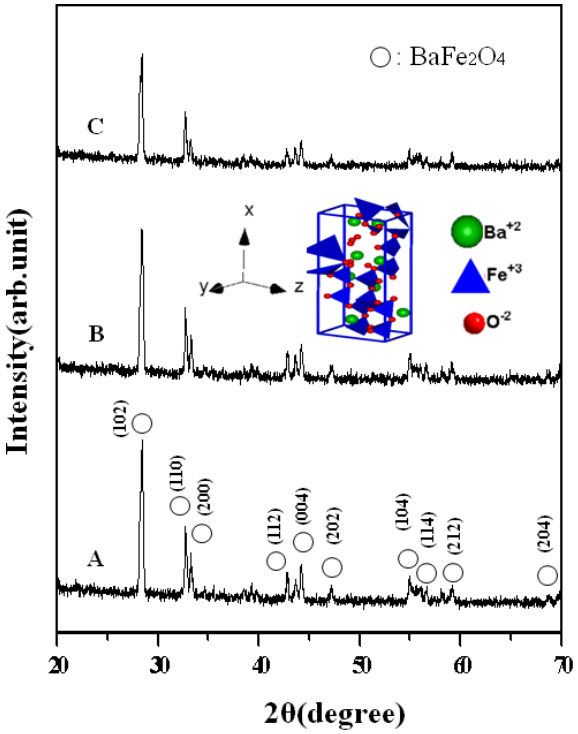

Fig. 1. (Color online) XRD patterns of $BaFe_2O_4$ samples calcined at (A) 1100, (B) 1200, and (C) 1300 °C.

III. RESULTS AND DISCUSSION

Structural characterization of the samples was carried out for phase identification, to estimate the particle size and to analyze the crystallization behavior of the samples prepared at various calcination temperatures. Figure 1 shows the XRD patterns of the samples calcined at various temperatures. An orthorhombic $BaFe_2O_4$ phase, as indicated by the open circles (see Fig. 1), was found to be formed at the temperatures ≥1100 °C. The cystallinity was found to increase with increasing calcination temperature, thereby retaining the pure phase (space group $Bb21m$) with lattice parameters as $a = 19.05$, $b = 5.39$, and $c = 8.4480$ Å. Higher crystallinity is well known to yield a high density of active catalytic sites, thereby yielding efficient photocatalysts [17].

Table 1. Crystallite size and band gap energy of $BaFe_2O_4$ particles prepared at various temperatures. $TiO_{2-x}N_x$ is included as reference system.

Catalyst	Temperature (°C)	Crystallite size (nm)	Band gap (eV)
$BaFe_2O_4$	1100	52.33	1.90
$BaFe_2O_4$	1200	52.21	1.85
$BaFe_2O_4$	1300	50.08	1.85
$TiO_{2-x}N_x$	400	13.2	2.76

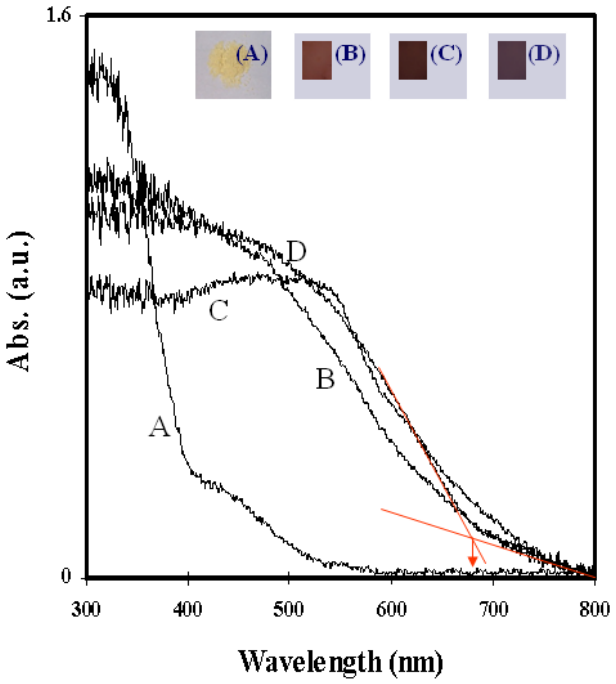

Fig. 2. (Color online) UV-Vis diffuse reflectance spectra of (A) $TiO_{2-x}N_x$; and $BaFe_2O_4$ calcined at: (B) 1100 °C, (C) 1200 °C, (D) 1300 °C. Inset shows the colors for respective samples.

Table 1 shows the crystallite sizes and the respective band gaps (described in next section) of the $BaFe_2O_4$ samples synthesized by calcination at different temperatures. The crystallite sizes were estimated from the full width at half maxima (FWHM) of the main XRD peak (Fig. 1) with a (212) orientation by using the Scherrer's equation [18]

$$D = 0.9\lambda/\beta\cos\theta, \quad (1)$$

Where λ is the wavelength of the X-ray radiation (Cu K_α with $\lambda = 1.54$ Å), β is the FWHM of the peak (in radians) corrected for instrumental broadening, θ is the Bragg angle, and D is the crystallite size (Å). The crystallite sizes for all the samples displayed in Fig. 1 are nearly the same (∼52 nm), revealing their nanocrystalline dimension.

Figure 2 shows the UV-vis diffuse reflectance spectra for $BaFe_2O_4$ prepared at 1100/1200/1300 °C and for the

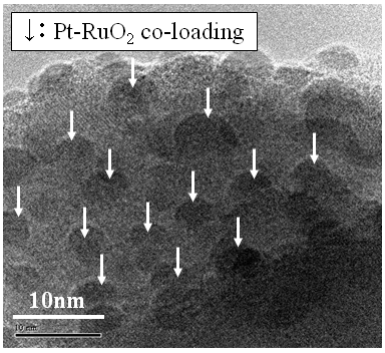

Fig. 3. HR-TEM image of Pt(0.5 wt%)/RuO_2(0.5 wt%) co-doped $BaFe_2O_4$ (calcined at 1300 °C. Pt was deposited on photocatalysts by using a photo-deposition method under visible light ($\lambda \geq 420$ nm). Arrows indicate the homogeneous existence of Pt over the photocatalyst.

$TiO_{2-x}N_x$ sample. From these spectra, we estimated the band gap energies of these materials as summarized in Table 1. The $BaFe_2O_4$ showed a clear absorption edge around a wavelength of ∼680 nm, yielding a band gap in the range of 1.8 - 1.9 eV. $TiO_{2-x}N_x$ showed two absorption edges, consisting of the main edge due to the oxide at 390 nm and another at 351nm due to the nitride [17]. The colors of these materials (see the inset of Fig. 2) were dark brown ($BaFe_2O_4$) and yellow ($TiO_{2-x}N_x$); thus, these materials, indeed, can absorb visible light. The band gap energies of the $BaFe_2O_4$ samples are greater than the theoretical energy required for water splitting ($\lambda > 1.23$ eV); thus, they are a suitable candidats for the role of a visible-light photocatalyst.

These samples were further used for photocatalytic characterization. Before the photocatalytic reaction, platinum nanoparticles and RuO_2 nanoparticles were deposited on all the $BaFe_2O_4$ samples. Figure 3 shows HR-TEM images demonstrating that well-dispersed ∼5 nm platinum/RuO_2 nanoparticles were deposited over the surfaces of the $BaFe_2O_4$ particles. It is noteworthy that the existence of a layered structure an observed in HRTEM is an additional advantage in a perovskite photocatalyst, being responsible for yielding enhanced photocatalytic sites.

To investigate the photodecomposition ability of the $BaFe_2O_4$ samples, we tested them for the photo-degradation of IPA and the photo-reduction of a water-methanol mixture under visible-light irradiation. Figure 4 shows the rate of CO_2 evolution, and Fig. 5 shows the amount of hydrogen evolution from the photo-catalytic reaction over the $TiO_{2-x}N_x$ and the $BaFe_2O_4$ samples. The concentration of CO_2 increased steadily with increasing irradiation time, indicating a rather larger decomposition rate of IPA under visible light irradiation for $BaFe_2O_4$ than for the oxynitride reference. The production of CO_2 gas stopped when light was turned OFF and restarted at the same rate when the light was turned ON again. The photocatalytic activity of $BaFe_2O_4$ for

Table 2. Photocatalytic H_2 gas evolution from a water-methanol mixture over various photocatalysts containing Pt (0.5 wt%) as a co-catalyst and RuO_2 (0.5 wt%) as a co-dopant on $BaFe_2O_4$.

Catalyst	Energy band gap E_g (eV)	H_2 evolution (mmol/gcat.hr)	
		UV light irradiation ($\lambda > 210$ nm)	Visible light irradiation ($\lambda > 420$ nm)
$Pt/BaFe_2O_4$	1.85	35	4
$Pt/RuO_2/BaFe_2O_4$	1.85	47	13
$Pt/TiO_{2-x}N_x$	2.74	9	Trace

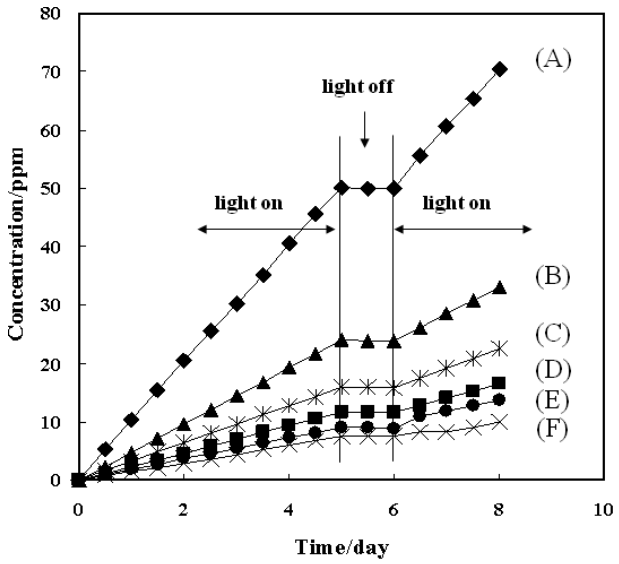

Fig. 4. Time courses of CO_2 evolution from IPA decomposition over various materials under visible light irradiation ($\lambda \geq 420$ nm) in the presence of 0.3 g of photocatalyst: (A) Pt(0.5 wt%)/RuO_2 (0.5 wt%) co-doped $BaFe_2O_4$, (B) Pt (0.5 wt%)/$BaFe_2O_4$, (C) Pt (0.5 wt%)/N-doped TiO_2, (D) $BaFe_2O_4$, (E) RuO_2 (0.5 wt%)/$BaFe_2O_4$, and (F) N-doped TiO_2. The IPA concentration was 200 ppm in air.

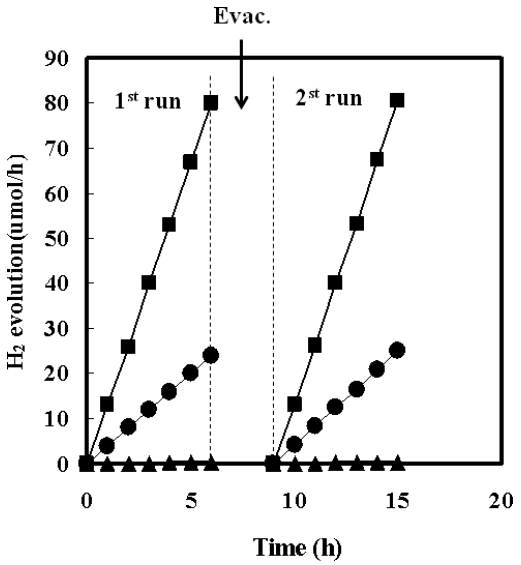

Fig. 5. Time courses for the photocatalytic reaction over various samples under visible light irradiation ($\lambda \geq 420$ nm) in an aqueous solution by stirring 0.3 g of photocatalyst. H_2 evolution: (-■-): Pt (0.5 wt%)/RuO_2 (0.5 wt%) co-doped $BaFe_2O_4$, (-●-): Pt (0.5 wt%)/$BaFe_2O_4$, and (-▲-) : Pt (0.5 wt%)/N-doped TiO_2.

IPA decomposition was about 4 times higher than that of $TiO_{2-x}N_x$. This clearly demonstrated the superiority of $BaFe_2O_4$ over the oxynitride reference photocatalyst. Further, as shown in Fig. 5, the H_2 production over $Pt/RuO_2/BaFe_2O_4$ was highest, and it was lowest in the case of the oxynitride sample. In all cases, the H_2 production steadily increased with increasing reaction time. The photo reactor was evacuated for 5 h before the next run to remove the gaseous products from the gas phase. Interestingly, the H_2 evolution rate was found to be reproducible in the following run. It can be concluded that H_2 evolution over these particles occurred photocatalytically. The photocatalytic quantum yield (QY) of the photocatalyst was calculated using the following equation [19,20]:

$$QY = H_2 \text{ evolution rate}/12.639 \times [(I_1 - I_3) - (I_1 - I_2)] \times A_1/A_2 \times 100 \qquad (2)$$

where I_1 is the blank light intensity, I_2 is the scattered light intensity, I_3 is the photocatalyst light intensity, A_1 is the lighted area of the photo reactor, A_2 is area of the sensor face, and 12.639 is the mole number of photons with $\lambda \geq 420$ nm emitted from the lamp for 1 h. The estimated quantum yields (QY) of ferrite samples were interestingly high, for the samples displayed in Table 2. Further studies were carried out for two different photon sources, one being under UV light and other being under visible light. Under UV light, all samples displayed significant QY for H_2 production (respective Table 2 samples QY ∼4.65, 6.24, and 1.2%). Under visible-light photon irradiation, only the $BaFe_2O_4$ samples yielded a significant QY value (∼1.73%) and a trace an hydrogen evolution for oxynitride sample. The enhanced photocatalytic QY of the $Pt/RuO_2/BaFe_2O_4$ sample is the important achievement in the present study.

To understand the photocatalytic performance of the new modified $BaFe_2O_4$, we propose a mechanism based on the results of our physical and physico-chemical studies. Accordingly, the schematic diagram shown in

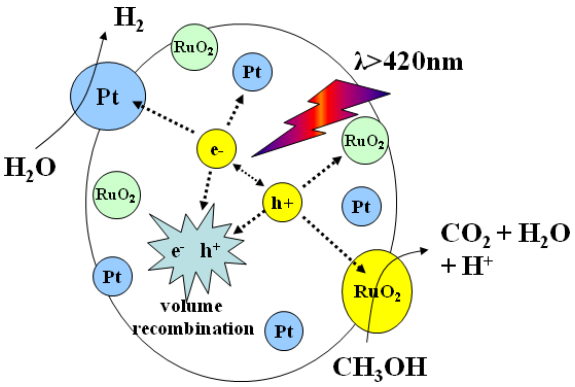

Fig. 6. (Color online) Schematic diagram explaining the mechanism of photodecomposition of iso-popanol and water over the modified photocatalyst of $Pt/RuO_2/BaFe_2O_4$.

Fig. 6 describes the possible reason behind the IPA photodegradation over modified $BaFe_2O_4$. In addition to the suitable band energetics of a base photocatalyst *viz.* $BaFe_2O_4$, the role of the co-catalyst [3,21] loading (here Pt and RuO_2) is a crucial step in the present study. This can be understood in the following way: The loading of a co-catalyst over the base photocatalyst enhances the efficiency because (i) RuO_2 assist in maintaining the charge separation of photo-generated *e*-*h* pairs and (ii) Pt, in turn, favors charge transfer to the electrolyte, thereby facilitating the desired reaction. In addition to the above co-catalyst effects, the higher optical response of $BaFe_2O_4$ in comparison to the optical response of the oxy-nitride reference further contributes towards the enhanced photocatalytic activity. The above study clearly demonstrates the superiority of the modified $BaFe_2O_4$ photocatalyst over $TiO_{2-x}N_x$ for the photo-degradation of IPA under visible-light photons and for the photo-reduction of water.

IV. CONCLUSION

The crystalline $BaFe_2O_4$ system, exhibiting an orthorhombic phase, was synthesized by using a solid state reaction method and was used for the photo-degradation of iso-propanol and for the photo-reduction of water under visible light irradiation. A pure orthorhombic phase was exhibited by $BaFe_2O_4$ at 1100 °C, which displayed a band gap of ∼1.9 eV (652 nm). The photocatalytic activity of $Pt/RuO_2/BaFe_2O_4$ for the photo-decomposition of isopropyl alcohol (IPA) and H_2 evolution under visible light (≥420 nm) was found to be significantly better than that for an oxynitride photocatalyst. This upgraded activity is correlated with the existence of suitable co-catalysts, the photochemical properties and the optical response of $BaFe_2O_4$ as compared to $TiO_{2-x}N_x$.

ACKNOWLEDGMENTS

This work has been supported by a Korea Basic Science Institute grant (T30320) and by the Hydrogen Energy R&D Center, Korea.

REFERENCES

[1] H. G. Kim, D. W. Hwang and J. S. Lee, J. Am. Chem. Soc. **126**, 8912 (2004).
[2] K. Maeda, T. Takata, M. Hara, N. Saito, Y. Inoue, H. Kobayashi and K. Domen, J. Am. Chem. Soc. **127**, 8286 (2005).
[3] Z. Zou, J. Ye, J. Sayama and H. Arakawa, Nature **424**, 625 (2002).
[4] G. Hitoki, T. Takata, J. Kondo, M. Hara, H. Kobayashi and K. Domen, Chem. Commun. **16**, 1698 (2002).
[5] R. Asahi, T. Ohwaki, K. Aoki and Y. Taga, Science **293**, 269 (2001).
[6] S. U. M. Khan, M. Al-Shahry and W. B. Jr. Ingler, Science **297**, 2243 (2002).
[7] S. Sakthivel and H. Kisch, Angew. Chem. Int. Ed. **42**, 4908 (2003).
[8] A. Ishikawa, T. Takata, J. N. Kondo, M. Hara, H. Kobayashi and K. Domen, J. Am. Chem. Soc. **124**, 13547 (2002).
[9] J. S. Jang, P. H. Borse, J. S. Lee, S. H. Choi and H. G. Kim, J. Chem. Phys. **128**, 154717 (2008).
[10] J. S. Jang, H. G. Kim, P. H. Borse and J. S. Lee, Int. J. Hydrogen Energy **32**, 4786 (2007).
[11] J. S. Jang, H. G. Kim, U. A. Joshi, J. W. Jang and J. S. Lee, Int. J. Hydrogen Energy **33**, 5975 (2008).
[12] H. G. Kim, P. H. Borse, W. Choi and J. S. Lee, Angew. Chem. Int. Ed. **44**, 45859 (2005).
[13] H. G. Kim, E. D. Jeong, P. H. Borse, S. Jeon, K. Yong, J. S. Lee, W. Li and S. H. Oh, Appl. Phys. Lett. **89**, 064103 (2006).
[14] J. S. Jang, D. W. Hwang and J. S. Lee, Catal. Today **120**, 174 (2007).
[15] R. A. Candeia, M. A. F. Souza, M. I. B. Bernardi, S. C. Maestrelli, I. M. G. Santos, A. G. Souza and E. Longo, Ceram. Int. **33**, 521 (2007).
[16] E. D. Jeong, P. H. Borse, J. S. Jang, J. S. Lee, C. R. Cho, J. S. Bae, S. Park, O. S. Jung, S. M. Ryu, M. S. Won and H. G. Kim, J. Nanosci. Nanotechnol. **9**, 3568 (2009).
[17] J. S. Jang, H. G. Kim, S. M. Ji, S. W. Bae, J. H. Jung, B. H. Shon and J. S. Lee, J. Solid State Chem. **179**, 1067 (2006).
[18] B. D. Cullity, *Elements of X-ray Diffraction*, 2nd ed. (Addison-Wesley Publishing Company, Inc., Reading, MA, 1978).
[19] S. W. Bae, P. H. Borse, S. J. Hong, J. S. Jang, J. S. Lee, E. D. Jeong, T. E. Hong, J. H. Yoon, J. S. Jin and H. G. Kim, J. Korean Phys. Soc. **51**, S22 (2007).
[20] S. J. Hong, P. H. Borse, S. M. Ji, J. S. Jang, J. S. Lee, E. D. Jeong, H. G. Kim and H. K. Park, J. Korean Phys. Soc. **51**, S27 (2007).
[21] H. Kadowaki, J. Sato, H. Kobayashi, N. Saito, H. Nishiyama, Y. Simodaira and Y. Inoue, J. Phys. Chem. B **109**, 22995 (2005).